Mon. Not. R. Astron. Soc. **362,** 592–608 (2005) doi:10.1111/j.1365-2966.2005.09337.x

A model for the infrared dust emission from forming galaxies

Tsutomu T. Takeuchi,[1⋆]† Takako T. Ishii,[2]‡ Takaya Nozawa,[3] Takashi Kozasa[3] and Hiroyuki Hirashita[4,5,6]‡

[1]*Laboratoire d'Astrophysique de Marseille, Traverse du Siphon BP8, 13376 Marseille Cedex 12, France*
[2]*Kwasan Observatory, Kyoto University, Yamashina-ku, Kyoto 607–8471, Japan*
[3]*Division of Earth and Planetary Sciences, Hokkaido University, Sapporo 060–0810, Japan*
[4]*Division of Particle and Astrophysical Sciences, Nagoya University, Nagoya 464–8602, Japan*
[5]*SISSA-ISAS, International School for Advanced Studies, Via Beirut 4, 34014 Trieste, Italy*
[6]*Center for Computational Sciences, University of Tsukuba, Tsukuba, Ibaraki 305–8577, Japan*

Accepted 2005 June 20. Received 2005 June 17; in original form 2005 February 14

ABSTRACT

Dust plays various important roles in galaxy formation and evolution. In the early epoch of galaxy evolution, dust is only supplied by supernovae (SNe). With the aid of a new physical model of dust production by SNe developed by Nozawa et al. (N03), we constructed a model of dust emission from forming galaxies on the basis of the theoretical framework of Takeuchi et al. (T03). N03 showed that the produced dust species depends strongly on the mixing within SNe. We treated both unmixed and mixed cases and calculated the infrared (IR) spectral energy distribution (SED) of forming galaxies for both cases. Our model SED is less luminous than the SED of T03 model by a factor of 2–3. The difference is due to our improved treatment of the ultraviolet (UV) photon absorption cross-section, as well as the different grain size and species newly adopted in this work. The SED for the unmixed case is found to have an enhanced near to mid-IR (N–MIR) continuum radiation in its early phase of the evolution (age $\lesssim 10^{7.25}$ yr) compared with that for the mixed case. The strong N–MIR continuum is due to the emission from silicon grains, which only exist in the species of the unmixed dust production. We also calculated the IR extinction curves for forming galaxies. N03 dust was found to yield a smaller extinction than that of T03 model. For the unmixed case, near-IR (NIR) extinction is dominated by large grains of silicon and amorphous carbon, and silicate features are less prominent compared to the curve given by T03. To the contrary, the extinction curve of the mixed case has a similar shape to that of T03. Then we calculated the SED of a local starbursting dwarf galaxy SBS 0335−052. Our present model SED naturally reproduced the strong N–MIR continuum and the lack of cold far-IR emission of SBS 0335−052. We found that only the SED of unmixed case can reproduce the NIR continuum of this galaxy. We then made a prediction for the SED of another typical star-forming dwarf, I Zw 18. The MIR continuum of I Zw 18 is expected to be much weaker than that of T03 SED. We also presented the evolution of the SED of Lyman-break galaxies. Finally, we discussed the possibility of observing forming galaxies at $z \gtrsim 5$.

Key words: dust, extinction – Galaxy: formation – galaxies: dwarf – galaxies: ISM – infrared: galaxies.

1 INTRODUCTION

In spite of the recent vast progress in both observational and theoretical studies, our understanding of the physics of galaxy formation and evolution is still far from sufficient.

The cosmic star formation (SF) history, introduced by Tinsley & Danly (1980) and developed by subsequent studies (e.g. Lilly et al. 1996; Madau et al. 1996), has always drawn much attention. Now the observations reach up to ∼6–8 (e.g. Stanway, Bunker & McMahon 2003; Bouwens et al. 2004a,b). In such studies, the role of dust has been increasingly recognized when we try to understand the evolution of galaxies in the context of cosmic SF history, because dust grains absorb stellar light and re-emit it in the far-infrared (FIR). Even a small amount of dust can lead to a significant underestimation of the SF rate (SFR) (Steidel et al. 1999; Adelberger & Steidel 2000).

⋆E-mail: tsutomu.takeuchi@oamp.fr
†Postdoctoral Fellow of the Japan Society for the Promotion of Science for research abroad.
‡Postdoctoral Fellow of the Japan Society for the Promotion of Science.

Indeed, there is another extreme category of high-z galaxies which have large amount of dust and are extremely luminous in the FIR and submillimetre (submm) wavelengths (e.g. Hughes et al. 1998; Eales et al. 2003). Heavily hidden SF is suggested in these galaxies (e.g. Takeuchi et al. 2001a,b; Totani & Takeuchi 2002).

Furthermore, from a physical point of view, dust grains are one of the fundamental ingredients in the activity of galaxies. As they are formed in a variety of environments ranging from explosive ejecta of novae and supernovae (SNe) to the outflowing gas of evolved low-mass stars, the dust formation is closely related to the SF activity (Dwek 1998). Moreover, the existence of dust is crucial in the physical process of galaxy formation and evolution through the formation of molecular hydrogen (e.g. Hirashita & Ferrara 2002). The dust itself plays a leading part in the physics of SF activity in galaxies in the whole period of the cosmic history.

Then, how about very young galaxies in the early Universe at $z \gtrsim 5$? It is often assumed, without deliberation, that the effect of dust is negligible for such young galaxies, because of their low metallicities. There is, however, a good counter-intuitive example in the local Universe: a local dwarf star-forming galaxy SBS 0335−052 has a very young stellar age ($\lesssim 10^7$ yr) and low metallicity ($1/41\,Z_\odot$), but has a heavily embedded active SF and strong continuum radiation in the near to mid-infrared (N–MIR) wavelength regime (Dale et al. 2001; Hunt, Vanzi & Thuan 2001). In addition, there are increasing number of observations suggesting the existence of dust in high-z systems such as Lyman α systems (e.g. Ledoux, Bergeron & Petitjean 2002; Ledoux, Petitjean & Srianand 2003) or quasi-stellar objects (e.g. Bertoldi et al. 2003).

To produce dust effectively in such a young system, the dust enrichment should have occurred primarily in the ejecta of SNe, especially Type II SN (SN II) explosions,[1] because the lifetime of the progenitor is short enough ($\sim 10^6$ yr) (e.g. Dwek & Scalo 1980; Kozasa, Hasegawa & Nomoto 1989). Recent theoretical studies claim the possibility of very massive stars for the first generation stars, which end their lives as pair-instability SNe (PISNe) (Heger & Woosley 2002; Umeda & Nomoto 2002). We should also take into account for the PISNe to study the very early evolution of dust. Recently, the dust formation in SNe ejecta has been observationally supported (e.g. Douvion et al. 2001; Morgan et al. 2003; Dunne et al. 2003).

For investigating the properties of dust in details, theoretical predictions for the amount and composition of dust are required. So far, some theoretical models of dust production by SNe have been developed. Todini & Ferrara (2001, hereafter TF01) showed that the dust mass produced by a SN II is 0.1–0.4 $M_\odot$ applying the theory of nucleation and grain growth by Kozasa & Hasegawa (1987). In the calculations, they assumed an adiabatic cooling in the ejecta with uniform gas density as well as elemental composition within the He core. They also found that SNe form amorphous carbon with size around 300 Å and silicate grains around 10–20 Å. Schneider, Ferrara & Salvaterra (2004) extended the progenitor mass range to the regime of PISNe (140–260 $M_\odot$) and found that 10–60 $M_\odot$ of dust forms per PISN. The grain radius depends on the species and is distributed from 0.001 to 0.3 μm.

Recently, (Nozawa et al. 2003) (hereafter N03) carefully took into account the radial density profile and the temperature evolution in the calculation of the dust mass in the ejecta of SNe II and PISNe. N03 showed that the produced dust species depends strongly on the mixing within SNe. In particular, carbon dust is not produced in the mixed case, because the carbon and oxygen are mixed and combined to form CO molecules. To the contrary, it forms in unmixed SN, as there is a carbon-rich region at a certain location in the ejecta of SNe. In addition, N03 predicts a dust mass larger than that of TF01 for SNe II.

The amount of dust produced in SNe is thus still a matter of debate. Morgan & Edmunds (2003) adopted a dust production smaller than those of TF01 or N03 in their theoretical calculation, in line with IR observations at the time. On the other hand, various observational efforts have been devoted to constrain the dust production efficiency of SNe (e.g. Arendt, Dwek & Moseley 1999; Dunne et al. 2003; Morgan et al. 2003; Green, Tuffs & Popescu 2004; Hines et al. 2004; Krause et al. 2004; Wilson & Batrla 2005). These results range from 0.003 $M_\odot$ to 1.0 $M_\odot$ per SN, and N03 dust production seems consistent with the upper range of these observational constraints. However, in these observational evaluations, a large uncertainty still remains due to the uncertainties in the estimation of dust mass in Cas A caused by the foreground contamination (Krause et al. 2004), although the evidence for dust in some SN remnants (SN1987A and Kepler) is still pointing towards SN origin. Thus, further close interaction between theoretical and observational works is required to overcome the uncertainties and obtain a reasonable picture of dust production in SNe.

In order to examine the dust properties of such high-z galaxies, the most direct observable is their spectral energy distribution (SED), especially at the FIR wavelengths. Hirashita, Hunt & Ferrara (2002) modelled the evolution of FIR luminosity and dust temperature in a young starburst on the basis of SNe II grain formation model of TF01. Takeuchi et al. (2003a) (T03) subsequently constructed a model of infrared (IR) SED of galaxies starting from the model of Hirashita et al. (2002). T03, for the first time, properly consider the dust size distribution peculiar to the very early stage of galaxy evolution in the model of the IR SED of very young galaxies, and successfully reproduced the peculiar MIR SED of SBS 0335−052 (though their result seems to have overestimated the FIR continuum). Takeuchi & Ishii (2004) (T04) applied the T03 model to the Lyman-break galaxies (LBGs). They found that the suggested hot dust in the LBGs (e.g. Ouchi et al. 1999; Chapman et al. 2000; Sawicki 2001) can be naturally explained by the T03 model.

As these works are based on TF01 conjecture, the dust formation model used is based on the classical nucleation theory (Feder et al. 1966). Recently, however, the importance of non-equilibrium (non-steady state) effects on the dust grain formation has been recognized in various astrophysical contexts (e.g. Gail, Keller & Sedlmayr 1984; Tanaka, Tanaka & Nakazawa 2002, N03). In addition, N03 found that the radial density profile of the SN progenitor and the temperature evolution of the ejecta also affect the dust grain formation. Hence, now is the time to take into account these concepts to further investigate the dust emission from young galaxies. In this work, we construct a new model of IR SED of extremely young galaxies based on N03 SN dust formation model. Starting from the size distribution and the amount of dust predicted by N03, we calculate the dust emission model by extending the T03 model to treat multiple dust species.

The paper is organized as follows. In Section 2 we explain the framework of our SED model. We present the basic result, the evolution of the SED of extremely young galaxies, in Section 3. Related discussions on local star-forming dwarf galaxies and high-z galaxies will be in Section 4. Section 5 is devoted to our conclusions. Throughout this paper, we use a cosmological parameter set of $(h, \Omega_0, \lambda_0) = (0.7, 0.3, 0.7)$, where $h \equiv H_0/100\,[\mathrm{km\,s^{-1}\,Mpc^{-1}}]$.

[1] More specifically, core-collapse SNe.

2 SED MODEL FOR FORMING GALAXIES

2.1 Species and size distribution of dust grains produced by SNe II

2.1.1 Dust production model of Nozawa et al. (2003) (N03)

N03 investigated the formation of dust grains in the ejecta of Population III SNe (SNe II and PISNe, whose progenitors are initially metal free). As we mentioned already, they treat some aspects which TF01 have not taken into account: (i) the time evolution of gas temperature is calculated by solving the radiative transfer equation including the energy deposition of radioactive elements; (ii) the radial density profile of various metals is properly considered; and (iii) unmixed and uniformly mixed cases in the He core are considered. In the unmixed case, the original onion-like structure of elements is preserved, and in the mixed case, all the elements are uniformly mixed in the helium core.

It should be mentioned here again that TF01 assumed an adiabatic cooling in the ejecta and adjusted the adiabatic index γ to 1.25, referring to the formation episode of dust grains observed in SN 1987A. As pointed out by Kozasa et al. (1989), the condensation time as well as the resulting average size of dust grains strongly depend on the value of γ. SN 1987A is somehow a peculiar SN in the sense that the progenitor is not a red supergiant but blue supergiant: see Arnett et al. (1989) for details. Using SN 1987A as a template may not be appropriate in comparisons to SNe as a whole. Therefore in this paper, we use the result of N03 as a standard model.

We should note that N03 also assume the complete formation of CO and SiO molecules, neglecting the destruction of those molecules, i.e. no carbon-bearing grain condenses in the region of $C/O < 1$ and no Si-bearing grain, except for oxide grains, condenses in the region of $Si/O < 1$. The formation of CO and SiO may be incomplete because of the destruction by energetic electron impact within SNe. TF01 treat both formation and destruction of CO and SiO, finding that both are mostly destroyed. The decrease of CO leads to the formation of carbon grains, which could finally be oxidized with available oxygen. The destruction of SiO could decrease the formation of grains composed of SiO_2, $MgSiO_3$ and Mg_2SiO_4, and increase other oxidized grains and silicon grains. Observationally, it is still a matter of debate if CO and SiO are efficiently destroyed or not. For the detailed discussions on this issue, see Appendix B of N03.

2.1.2 Dust grain species produced by the N03 model

In the unmixed ejecta, a variety of grain species (Si, Fe, Mg_2SiO_4, $MgSiO_3$, MgO, Al_2O_3, SiO_2, FeS and C) condense, and in the mixed ejecta, in contrast, only oxide grains (SiO_2, $MgSiO_3$, Mg_2SiO_4, Al_2O_3 and Fe_3O_4) form. This is because carbon atoms are consumed to form CO molecules. We summarize the species formed in SNe in Table 1, where the species marked with a circle are relevant for unmixed and mixed SNe. The size of the grains spans a range of three orders of magnitude, depending on the grain species. The size spectrum summed up over all the grain species has a very broad distribution, and very roughly speaking, it might be approximated by a power law. This size distribution is different from that of the SN II calculation of TF01, which has typical sizes of 300 Å for amorphous carbon and 10–20 Å for oxide grains.

In this work, we adopt the representative progenitor mass of SNe II as $20\,M_\odot$. N03 have shown that the size distribution of each grain species is almost independent of the progenitor mass, if the SN type is fixed (i.e. SN II or PISN). We examine the unmixed and mixed cases. The size distributions of dust grains in the mixed and unmixed cases calculated by N03 are shown in Fig. 1. We used these size distributions after binning with a bin width of 0.2 dex for our calculations. Throughout this work, we assume a uniform and spherical grain. It should be mentioned that a different shape of dust grains in SN is suggested (e.g. Dwek 2004).

Table 1. Dust grain species.

Species	Unmixed	Mixed	Density (ρ_i) ($g\,cm^{-3}$)	Ref.[a]
C	○		2.28	1
Si	○		2.34	2
SiO_2	○	○	2.66	3
Fe	○		7.95	4
FeS	○		4.87	5
Fe_3O_4		○	5.25	6
Al_2O_3	○	○	4.01	7
MgO	○		3.59	8
$MgSiO_3$	○	○	3.20	9
Mg_2SiO_4	○	○	3.23	5

[a]References for optical constants: (1) Edo (1985), (2) Edward (1985), (3) Philipp (1985), (4) Lynch & Hunter (1991), (5) Semenov et al. (2003), (6) Mukai (1989), (7) Toon, Pollack & Khare (1976), (8) Roessler & Huffman (1991), and (9) Dorschner et al. (1995).

2.2 SF, chemical evolution and dust production

For constructing the chemical evolution model of a young galaxy, we adopt the following assumptions.

(i) We use a closed-box model, i.e. we neglect an infall and outflow of gas in the scale of a star-forming region.

(ii) For the initial mass function (IMF), we adopt the Salpeter IMF (Salpeter 1955)

$$\phi(m) \propto m^{-2.35} \tag{1}$$

with mass range of $(m_1, m_u) = (0.1\,M_\odot, 100\,M_\odot)$.

(iii) We neglect the contribution of SNe Ia and winds from low-mass evolved stars to the formation of dust, because we consider the time-scale younger than 10^9 yr.

(iv) The interstellar medium is treated as one zone, and the growth of dust grains by accretion is neglected. Within the short time-scale considered here, it can be assumed safely (see, e.g. Whittet 1992, pp. 223–224).

(v) We also neglect the destruction of dust grains within the young age considered (see e.g. Jones, Tielens & Hollenbach 1996).

(vi) We assumed a constant SFR for simplicity.

using these assumptions, we calculate the chemical evolution. Details of the formulation are presented in Appendix A.

The evolution of the total dust amount for SFR $= 1\,M_\odot\,yr^{-1}$ is shown in Fig. 2. The dust mass fraction for unmixed and mixed cases are summarized in Tables 2 and 3, respectively. Comparing the evolution of dust mass given by T03, dust mass starts to accumulate later than the case of T03, and gradually approaches the T03 result towards the age of about 10^8 Gyr. This difference is caused by the different formulae we adopted in the calculations of stellar lifetime: the formula of Schaerer (2002) gives a longer lifetime for the same stellar mass than that of Inoue, Hirashita & Kamaya (2000) which is used in T03. At 10^8 Gyr, T03 and present work yield the same dust mass.

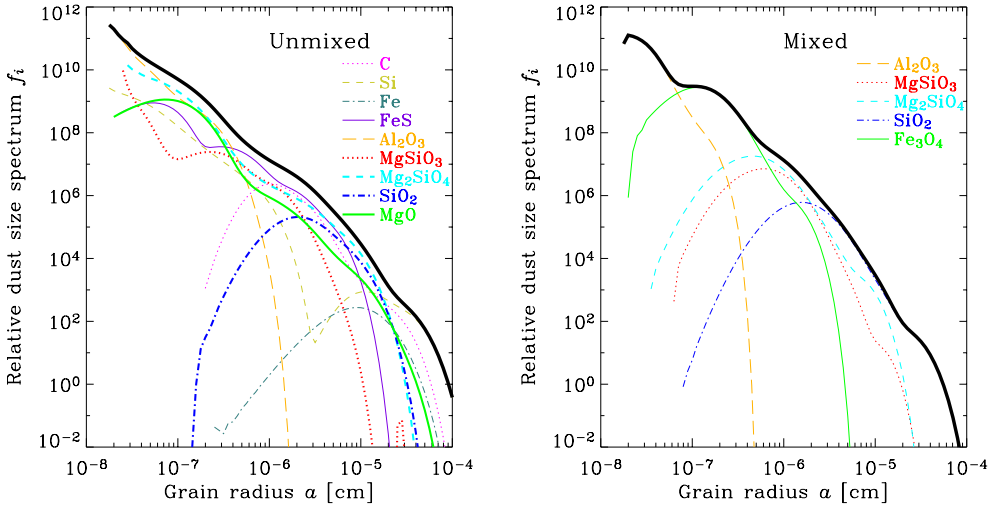

Figure 1. Dust size distributions of the SN II model with the progenitor mass of 20 $M_\odot$ by Nozawa et al. (2003). The thick lines are the total dust size distribution function. The labels 'unmixed' and 'mixed' indicate the adopted assumption of the mixing of elements in the ejecta. We assumed 20 $M_\odot$ as a representative for the SN progenitor mass in this work.

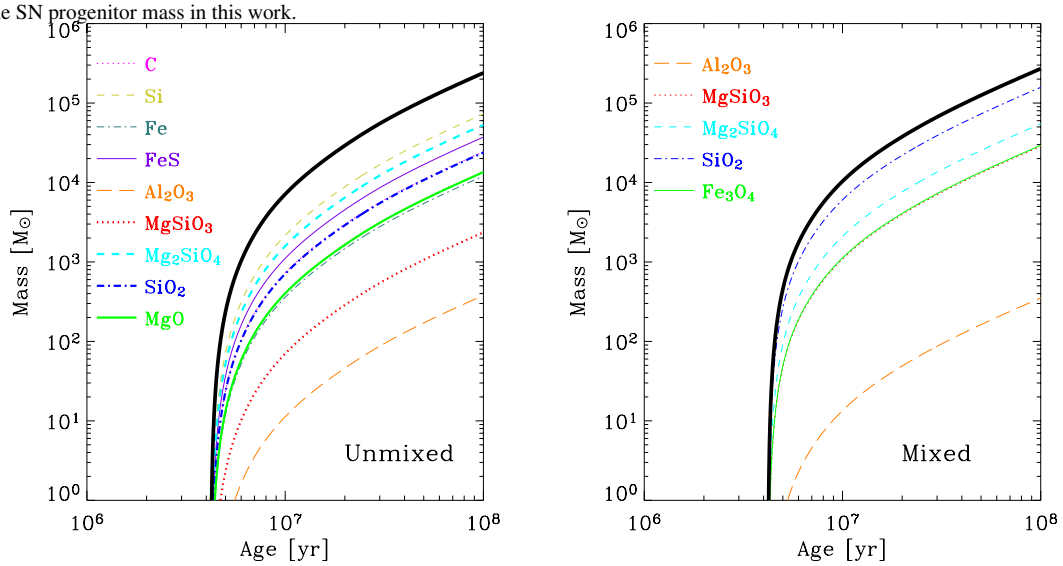

Figure 2. Evolution of the mass for each grain species. The thick lines indicate the total amount of dust mass. We assumed the closed-box model and a constant SFR. The mass fraction of each grain species is constant in time and is given by the size distribution function (Fig. 1).

Table 2. Mass fraction of dust species (unmixed).

Species	Mass fraction
C	0.102
Si	0.303
Fe	0.050
FeS	0.156
Al_2O_3	0.002
$MgSiO_3$	0.010
Mg_2SiO_4	0.222
SiO_2	0.099
MgO	0.056

Table 3. Mass fraction of dust species (mixed).

Species	Mass fraction
Al_2O_3	0.001
$MgSiO_3$	0.105
Mg_2SiO_4	0.202
SiO_2	0.583
Fe_3O_4	0.108

2.3 SED construction

In this subsection, we present the construction of the SED from dust. As most of the formulations are in parallel to those in T03 and T04, here we list the essence of our calculation.

(i) *Stochastic heating of very small grains*

Very small grains cannot establish thermal equilibrium with the ambient radiation field, which is called stochastic heating (e.g. Krügel 2003). To treat this effect, we applied the Debye model to the specific heat of the grain species as discussed in T03 and T04. We adopt a multidimensional Debye model (e.g. Draine & Li 2001) (DL01) for carbon (C) and silicate (SiO_2, $MgSiO_3$ and Mg_2SiO_4) grains. For other species, we adopt the classical

Table 4. The specific heat of each species.

Species	Debye temperature (K)	Ref[a]	$N_{\rm atom}$ (10^{22} cm^{-3})	$C(T)$ model[b]
C	863	1	11.4	Multi-Debye
Si	616	2	5.00	Debye
SiO_2	—	1	7.96	Multi-Debye
Fe	500	3	8.50	Debye
FeS	384	4	6.62	Debye
Fe_3O_4	511	5	28.4	Debye
Al_2O_3	1030	6	23.5	Debye
MgO	762	7	10.7	Debye
$MgSiO_3$	—	1	9.57	Multi-Debye
Mg_2SiO_4	—	1	9.63	Multi-Debye

[a]References for Debye temperatures: (1) Draine & Li (2001), (2) Oganov, Brodhold & Price (2000), (3) Siethoff & Ahlborn (1996), (4) Grønvold et al. (1991), (5) Shepherd et al. (1991), (6) Mezzasalma (2000), (7) Hama & Suito (1999).

[b]'Debye' means that the specific heat $C(T)$ is modelled by the classical Debye model, while 'Multi-Debye' means that the multidimensional Debye model proposed by Draine & Li (2001) is adopted. For the species to which we adopt the multidimensional Debye model, we do not give the classical Debye temperature.

three-dimensional Debye model with a single Debye temperature. The specific heat model is summarized in Table 4.

(ii) *Emission*

The emission from dust is calculated in the same way as T03/T04, basically according to Draine & Anderson (1985). Total dust emission is obtained as a superposition of the emission from each grain species. The total mass of each grain component is given by N03. With this value and material density of each species (Table 1), we can determine the normalization of the dust size distribution (see Appendix B).

We constructed $Q(a, \lambda)$ of each grain species from available experimental data via Mie theory (e.g. Krügel 2003, Chapter 2). The extinction efficiencies are presented in Fig. 3. T03 adopted Draine & Lee (1984) for the optical properties of these species, being different from the present work. In contrast, we treat detailed species in the present work. Hence, the mass fraction distributed to carbon and silicate are significantly reduced comparing to the case of T03. In the IR, $Q(a, \lambda)$ of these grains is much larger than other grains at the whole range of grain size. As a result, the sum of the contributions of all grains are less than that of the case where only two species are considered as T03.

(iii) *Extinction*

Self-absorption in the MIR for a very optically thick case is treated by a thin shell approximation, in the same manner as T04.

3 RESULTS

3.1 Evolution of IR SED

We first show the evolution of the IR SED of forming galaxies based on our baseline model. For these calculation we adopted SFR $= 1\,{\rm M}_\odot\,{\rm yr}^{-1}$. We adopt $r_{\rm SF} = 30$ and 100 pc, the same as those used in T03. These values are relevant when describing 'dwarf-like' young galaxies. The former successfully reproduce various properties of active star-forming dwarf galaxies like SBS 0335−052, whereas the latter is representative of the size of quiescent dwarf galaxies like I Zw 18 (Hirashita & Hunt 2004). We will revisit these representative dwarf starburst galaxies in Section 4.

The results are presented in Figs 4 and 5. Fig. 4 is the SED of a galaxy with $r_{\rm SF} = 30$ pc, while Fig. 5 is the one for $r_{\rm SF} = 100$ pc. We calculated the evolution of the SED in the age range of $10^{6.5}$ –10^{8} yr. In a very young phase (age $= 10^{6.75}$–$10^{7.25}$ yr), unmixed-case SED has an enhanced N–MIR continuum. After $10^{7.25}$ yr, the N–MIR continuum is extinguished by self-absorption in the case of $r_{\rm SF} = 30$ pc. In contrast, self-absorption is not significant for $r_{\rm SF} = 100$ pc.

In both cases, the SEDs have their peaks at a wavelength $\lambda \simeq 20$–30 μm, which is much shorter than those of dusty giant galaxies at $z = 1$–3 detected by Submillimetre Common User Bolometer Array (SCUBA). At submm wavelengths, the shape of the continuum is very similar to each other for mixed and unmixed cases, though the unmixed case predicts stronger fluxes by a factor of 2. This is explained by the grain size distributions of the unmixed and mixed cases: carefully examining Fig. 1, we see that the largest-size dust grains are more abundant for the unmixed-case size distribution. It means that larger grains contribute more significantly than smaller ones. As larger grains radiate their energy at longer wavelengths, the total SED has a stronger FIR-submm continuum.

As a whole, our model SEDs are less luminous than those of T03 by a factor of 2–3. This is due to the difference in considered grain species, and more importantly, also due to the improvement of the treatment of $Q(a, \lambda)$ at the ultraviolet (UV); $Q(a, \lambda)$ was approximated to be unity in T03. Also T03 treated the size dependence of $Q(a, \lambda)$ by a simple scaling law, which was not very accurate. As seen in Fig. 3, the size dependence of $Q(a, \lambda)$ cannot be described by a simple scaling law, especially at the MIR (see, e.g. Si, Fe and FeS). We, in this work, used the exact value of $Q(a, \lambda)$ in all the wavelengths. As some elements have a very small value for $Q(a, \lambda)$ at the UV regime, the total absorption probability of UV photons is smaller than that of T03. A strong N–MIR continuum at a very young phase and the dependence on $r_{\rm SF}$ are qualitatively consistent with the previous result of T03. However, the dust grains expected from the N03 model predict a peak of the SED at shorter wavelengths than those of T03. In addition, a relatively small amount of small dust grains also makes the N–MIR SED weaker than the T03 one.

3.2 Contribution of each species to the SED

The dust species treated here are much more detailed than those of T03. In order to see the detailed contributors to the total SEDs, we show the individual SED of each species in Fig. 6. We show the SED with the age of burst $10^{6.75}$ yr, where the effect of self-absorption is negligible.

In both the unmixed and the mixed cases, the smallest dust grain species is Al_2O_3 (Fig. 1). However, because of its small fraction in mass (Fig. 2), Al_2O_3 contributes to the total SED very little. The main contributor to the (unextinguished) N–MIR continuum is silicon for unmixed case and Fe_3O_4 in mixed case, respectively. These species are the second smallest grains. For the unmixed case, as the emissivity of silicon grains with the size of $\sim 10^{-7}$ cm is much smaller than that of Fe_3O_4 at $\lambda \gtrsim 1$ μm, the grain temperature becomes much higher than that of Fe_3O_4, which makes the very strong N–MIR continuum emission. In contrast, as $Q(a, \lambda)$ of Fe_3O_4 is large, the resultant SED for the mixed case does not have a strong N–MIR continuum.

At $\lambda = 10$–20 μm, several species contribute equally to the SED in unmixed case, while SiO_2 play a dominant role for mixed case. At longer wavelengths, the main contributors to the SED are Mg_2SiO_4 and amorphous carbon for the unmixed case, and $MgSiO_3$ and Mg_2SiO_4 in the mixed case. In addition, especially at $\lambda \gtrsim 200$ μm, FeS (unmixed) and Fe_3O_4 (mixed) are also important

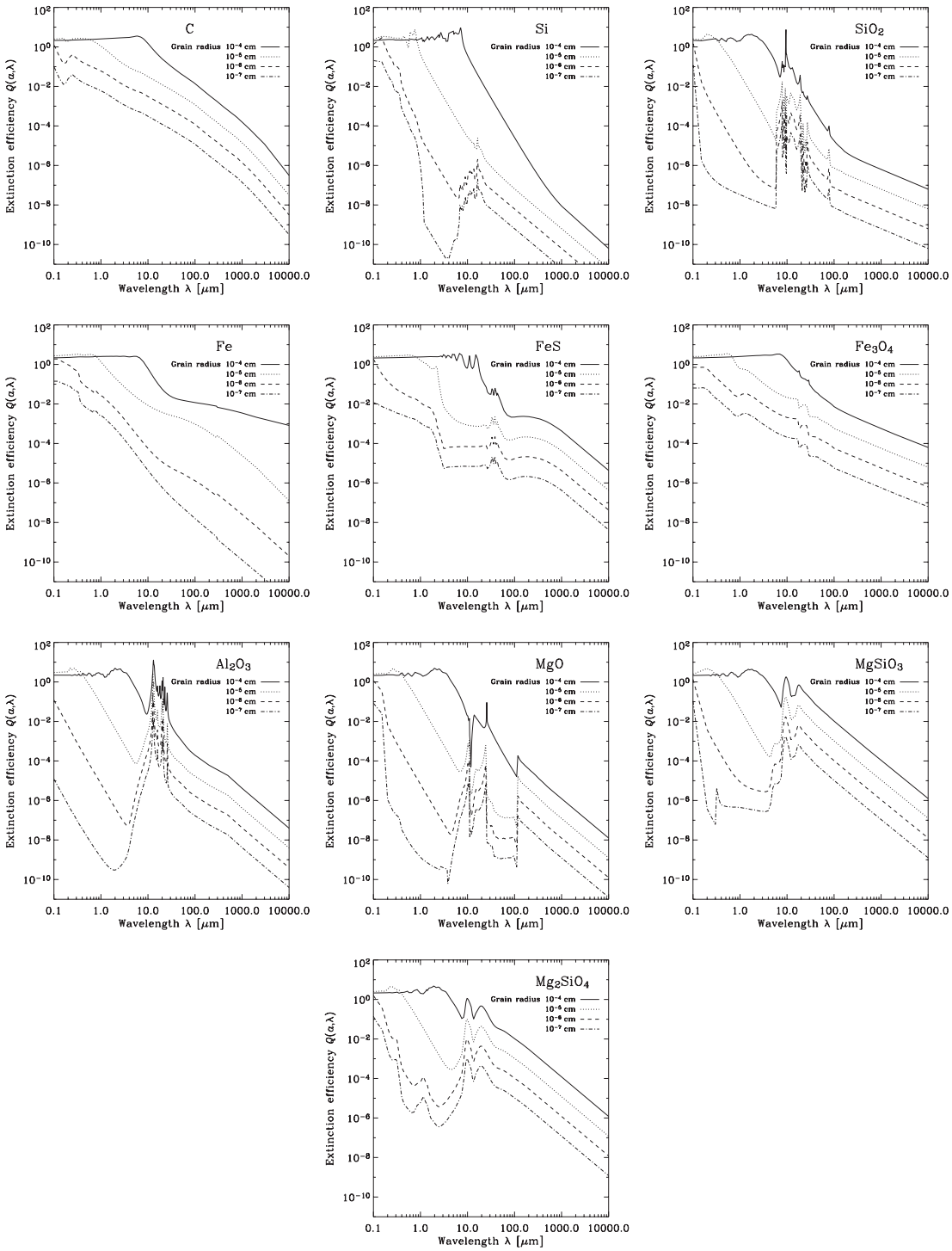

Figure 3. Extinction efficiency $Q(a, \lambda)$ for the grain species produced by the SN model of Nozawa et al. (2003). We show $Q(a, \lambda)$ for the radius $a = 10^{-7}$, $10^{-6}, 10^{-5}$ and 10^{-4} cm by the curves from bottom to top in each panel.

because of their shallow slope of the extinction efficiency at the longer wavelength regime. Note that, for the mixed case, Fe_3O_4 contribute to both NIR and FIR.

3.3 Opacity and its evolution

The extinction curve A_λ is obtained as

$$A_\lambda = 1.086\tau_{\rm dust}(\lambda). \quad (2)$$

In this work we concentrate on the extinction curve in the IR. Detailed discussions of the extinction curves in the optical wavelength regime are given in Hirashita et al. (2005).[2]

[2] As we assume a very simple geometry, the extinction curve is directly related to the 'attenuation curve', in which the geometrical effect is also included (for a thorough discussion on this subject, see, e.g. Inoue 2005).

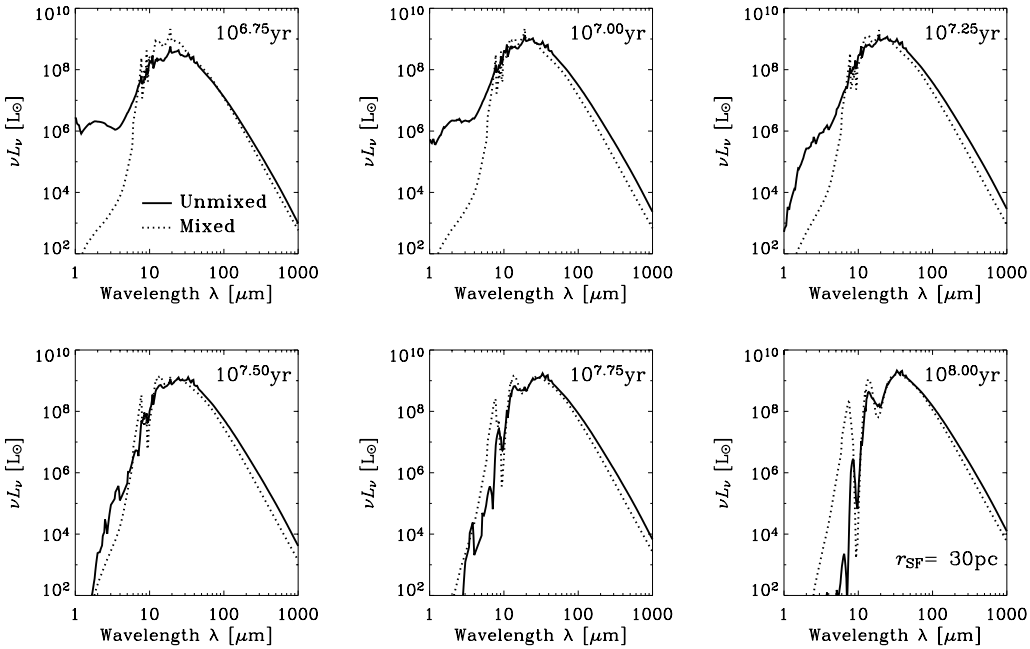

Figure 4. The evolution of the IR SED of a very young galaxy. The size of the star-forming region, r_{SF}, is 30 pc. Solid and dotted lines represent the SEDs based on the unmixed and mixed model of dust production (Nozawa et al. 2003), respectively. For Figs 4 and 5, a constant SFR of SFR $= 1\,M_\odot\,yr^{-1}$ is adopted.

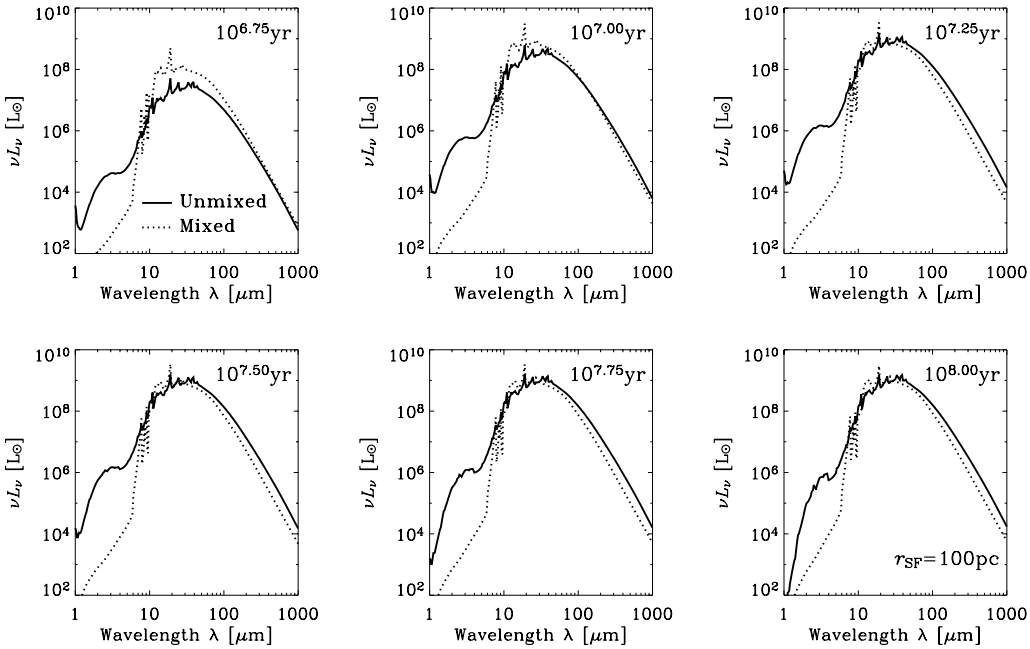

Figure 5. Same as Fig. 4, but the size of the star-forming region, r_{SF}, is 100 pc.

Fig. 7 presents the evolution of the IR opacity for a young galaxy with the age of $10^{6.75}$–10^8 yr (from the bottom to the top). In the case of $r_{SF} = 30$ pc, the extinction becomes almost unity at 10 μm when the age is $10^{7.25}$ yr. Hence, after this age, the N–MIR regime of the SED becomes optically thick, and this makes the continuum extinguished in Fig. 4. On the other hand, for $r_{SF} = 100$ pc, it remains optically thin even at the age of 10^8 yr at 10 μm.

In Fig. 7, we find an interesting difference between the extinction curves of the unmixed and mixed cases. Though their behaviour is similar to each other at wavelengths $\lambda \gtrsim 10$ μm, there is no dip at $\lambda \lesssim 10$ μm in the curve of the unmixed case. This makes the extinction stronger for the unmixed-case galaxies at N–MIR. In addition, the MIR bumps at 10 and 20 μm are less prominent for the unmixed case.

Comparing these IR extinction curves with the T03 model, we find that the amount of the extinction is smaller than that of T03 by a factor of 2–10, depending on the wavelength and unmixed/mixed production. This is explained by the discussion presented in

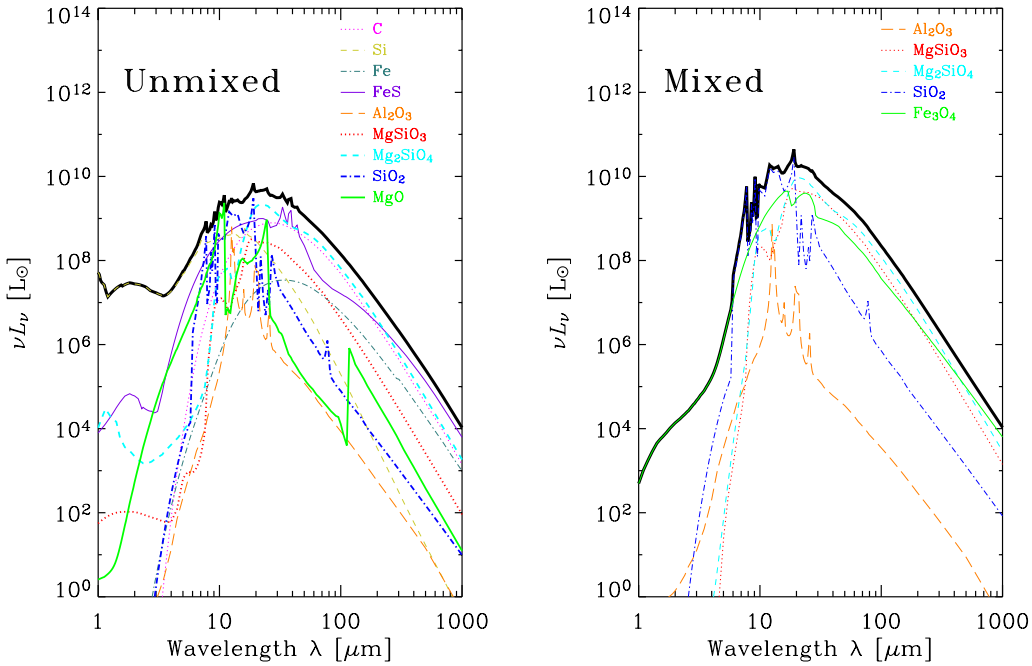

Figure 6. The contribution of each dust species to the total SED of a young galaxy. In this figure we set the galaxy burst age to be $t = 10^{6.75}$ yr and the radius of the star-forming region to be $r_{\rm SF} = 30$ pc. The left panel is the SED calculated from the unmixed dust production, and the right panel is obtained from the mixed dust production.

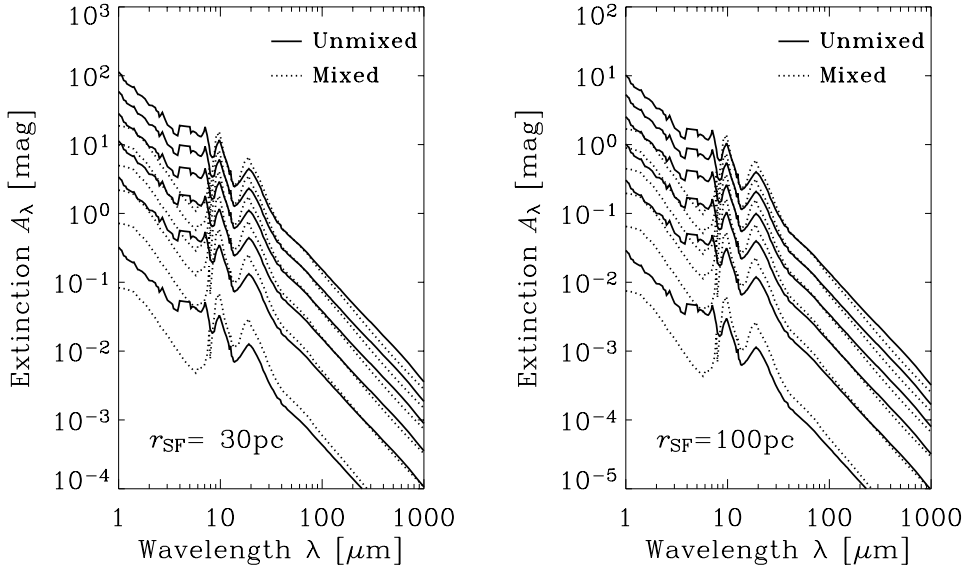

Figure 7. The evolution of the opacity of a very young galaxy at IR wavelengths. The left panel shows the IR extinction curves calculated with the star-forming region size $r_{\rm SF} = 30$ pc, and the right panel shows the curves with $r_{\rm SF} = 100$ pc. From the bottom to the top, the ages of galaxies are $10^{6.75}$, $10^{7.0}$, $10^{7.25}$, $10^{7.5}$, $10^{7.75}$ and $10^{8.0}$ yr, respectively. The solid and dashed curves represent the IR extinction curves based on the unmixed and mixed model, respectively.

Section 2.3: T03 supposed silicates and carbon grains as the constituents of dust grains from SNe. As their $Q(a, \lambda)$ is larger than the other species predicted by N03, the total extinction becomes smaller in this work.

As for the shape of the curve, the extinction curve for the mixed model resembles that of T03 extinction curves, while the curve for the unmixed model is qualitatively different at MIR, because of the weak MIR bump features and the lack of the MIR dip mentioned above.

Fig. 8 demonstrates the contribution of each dust grain species to the total IR extinction curves. The adopted age is 10^7 yr as a representative, but the contribution is constant with time.

For the extinction curve of the unmixed case, bump features at MIR are relatively weak (Fig. 7). Similar to those of the Galactic IR extinction curve, they are due to silicate grains. In the unmixed-model extinction, the bumps are dominated by Mg_2SiO_4, and the contribution from $MgSiO_3$ is not important. We also find a strong contribution from amorphous carbon grains which have very smooth

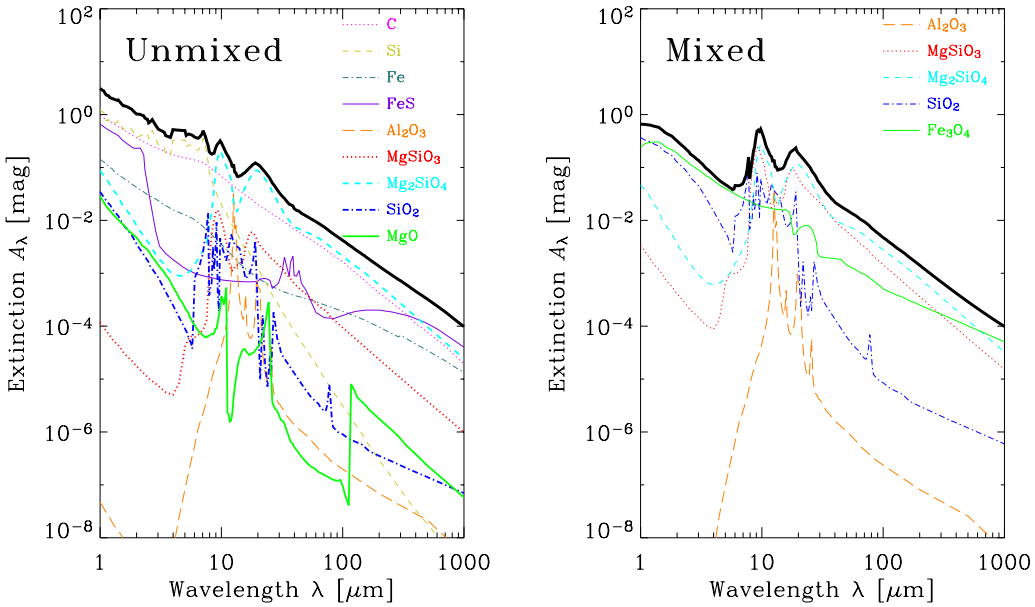

Figure 8. The contribution of each dust species to the total IR extinction curve of a young galaxy. In this figure we set the galaxy burst age of $t = 10^7$ yr. The left panel is the extinction curve calculated from the unmixed dust production, and the right panel is obtained from the mixed dust production.

dependence of $Q(a, \lambda)$ on wavelength. They makes the silicate features rather weak, because of their comparable contribution with Mg_2SiO_4. We note that the amorphous carbon does not have any dip at $\lambda \simeq 5$–10 μm. Further, large grains of silicon have a large $Q(a, \lambda)$ at these wavelength regime. We find that both the amorphous carbon and the silicon grains equally contribute to the total extinction at N–MIR, and these species plug up the MIR dip of Mg_2SiO_4. At NIR wavelengths close to 1 μm, FeS also contributes to the total extinction.

We next see the mixed case. In this case, $MgSiO_3$ and Mg_2SiO_4 equally contribute to the total extinction around the MIR bumps. In contrast to the unmixed case, there is no species which fill up the dip of silicates, hence we see clear silicate bump features and dips in the IR extinction curve. In the N–MIR, the main contributors to the opacity are Fe_3O_4 and SiO_2. The contribution from Al_2O_3 is not important at any wavelength.

4 DISCUSSION

4.1 Nearby forming dwarf galaxies

It is still a difficult task to observe galaxies in the very first phase of the SF, especially to detect their dust emission directly. Along the line of studies made by Hirashita et al. (2002), T03 considered two local star-forming dwarf galaxies, SBS 0335−052 and I Zw 18, for investigating the dust emission from very young small galaxies. Here we revisit these representative star-forming dwarfs with our framework. As a recent observation of SBS 0335−052 by *Spitzer* has been reported (Houck et al. 2004), it is timely to reconsider these 'textbook objects' with the new data. In addition, understanding the SEDs of these objects will shed light to the physics of interstellar matter and radiation of high-z galaxies also via empirical studies (e.g. Takeuchi, Yoshikawa & Ishii 2003b; Takeuchi et al. 2005).[3]

4.1.1 SBS 0335−052

SBS 0335−052 is a local galaxy (∼54 Mpc) with SFR $= 1.7\,M_\odot\,yr^{-1}$ (Hunt et al. 2001) and extremely low metallicity $Z = 1/41\,Z_\odot$. This galaxy is known to have an unusual IR SED and strong flux at N–MIR. It has a very young starburst (age $\lesssim$ 5 Myr) without a significant underlying old stellar population (Vanzi et al. 2000). T03 have modelled the SED of SBS 0335−052 and reported good agreement with the available observations at that time.

However, Houck et al. (2004) presented new data of the MIR SED by *Spitzer*, and reported a deviation of the model by a factor of 2 or 3. Their observation indicated that SBS 0335−052 has even more FIR-deficient SED than ever thought. Hence, it is interesting to examine whether our present model can reproduce the extreme SED of this galaxy. We are also interested in the possibility to determine which of the two pictures, unmixed or mixed, is plausible, by a direct measurement of the SED.

We show the model SEDs for SBS 0335−052 in Fig. 9. We have calculated the SED for $r_{SF} = 10$, 20 and 30 pc for both unmixed and mixed cases. The SFR is fixed to be $1.7\,M_\odot\,yr^{-1}$, and the age is $10^{6.5}$ yr. The solid squares are the observed data from the *Infrared Space Observatory ISO*, while open squares represent the upper limits obtained from *IRAS* and *ISO* observations. The open triangles are the expected contribution of dust emission calculated by the recipe of Joy & Lester (1988). The filled triangles depict the measured SED of SBS 0335−052 by *Spitzer* IRS taken from Houck et al. (2004) in the MIR. The filled triangle at FIR is the estimate from the radio observation of Hunt et al. (2004), which is used by Houck et al. (2004). Details of the other observational data are found in Section 4 of T03.

In the FIR regime, our model SEDs are consistent with the strong constraint given by Houck et al. (2004), both for the unmixed and mixed cases. This is because our present model predicts a peak of

[3] We should keep in mind that the following discussion is limited to a particular class of dwarf galaxies dominated by newly formed stars. For the modelling of the SED of normal star-forming dwarfs, see, e.g. Galliano et al. (2003, 2005).

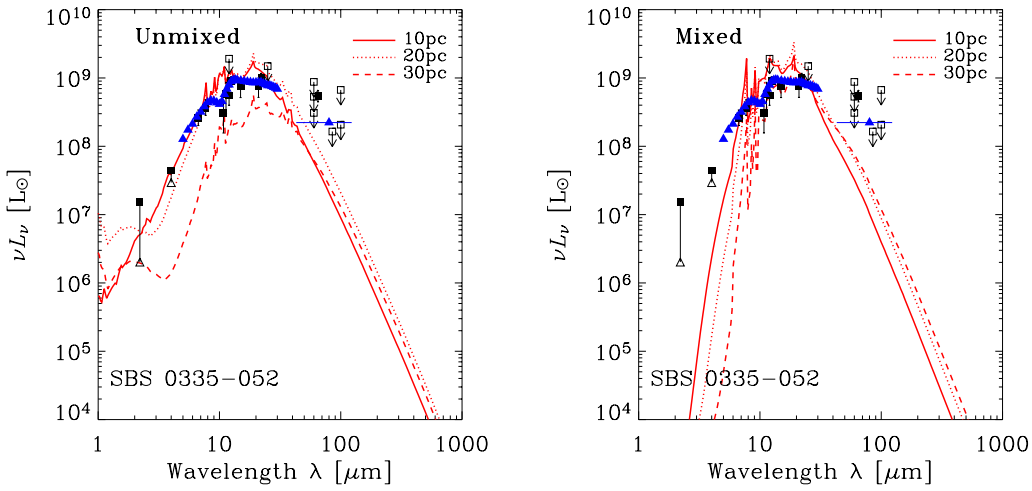

Figure 9. The model for the SED of a nearby star-forming dwarf galaxy SBS 0335−052. We adopt the SFR SFR = 1.7 M$_\odot$ yr^{-1} (Hunt et al. 2001). The galaxy burst age is found to be $t = 10^{6.5}$ yr and the radius of the star-forming region is set at $r_{\rm SF} = 10$, 20 and 30 pc. Solid squares are the observed data from *ISO*, while open squares represent the upper limits obtained from *IRAS* and *ISO* observations. Open triangles are the expected contribution of dust emission calculated by the recipe of Joy & Lester (1988). Solid triangles are taken from recent observation of SBS 0335−052 by *Spitzer* (Houck et al. 2004). The left panel is the SED calculated from the unmixed dust production, and the right panel is obtained from the mixed dust production. Clearly, the mixed dust production poorly reproduces the observed SED of SBS 0335−052.

the SED at shorter wavelengths than that of T03. At MIR, though we cannot give an excellent fit to the observed data, the model SEDs roughly agree with them, and the unmixed-case SEDs with $r_{\rm SF} =$ 10–20 pc give a better fit. The very strong N–MIR continuum of SBS 0335−052 is well reproduced by the SED of the unmixed dust production picture. In contrast, the SEDs of the mixed case seriously underpredicts the observationally suggested N–MIR continuum. As we can also calculate the extinction value A_λ, we can distinguish between a mixed-case SED and heavily extinguished unmixed SED without ambiguity.

In summary, the SED for the unmixed dust production with $r_{\rm SF} =$ 10–20 pc yields a reasonable fit to the latest observations by *Spitzer*. This result suggests that we may determine the dust production (unmixed or mixed) of SNe through the observation of the N–MIR SEDs of forming galaxies. As for SBS 0335−052, the unmixed dust production is suggested to take place. In a previous work, we have modelled a high-z ($z = 6.2$) extinction curve (Maiolino et al. 2004) and found that it is well represented by dust produced in unmixed SNe (Hirashita et al. 2005). This conclusion is strengthened by our earlier result.

The dust mass calculated by our model at this age of SBS 0335−052 is 1–2 × 10^3 M$_\odot$, consistent with the observationally estimated value by Dale et al. (2001). We note that the mass estimation is strongly dependent on the assumed dust species and their emissivities, and grain size distribution. As we discussed in Section 3, the continuum radiation in the N–MIR is dominated by stochastically heated dust emission, which is completely different from a modified blackbody. Therefore, when we try to estimate the dust mass, we must take care to determine the corresponding grain properties, i.e. radiative processes and grain which are related to the observed SED of galaxies.

4.1.2 I Zw 18

I Zw 18 is the most metal-deficient star-forming galaxy in the local Universe ($Z = 1/50\,{\rm Z}_\odot$). We adopt its distance of 12.6 Mpc (Östlin 2000), and the SFR of 0.04 M$_\odot$ yr^{-1}. The existence of the underlying old stellar population is suggested for this galaxy, but their contribution is not dominant (Hunt, Thuan & Izotov 2003). Thus, it is not unreasonable to adopt our present model to predict the IR SED of I Zw 18.

Cannon et al. (2002) estimated the total dust mass $M_{\rm dust} = 2$–3×10^3 M$_\odot$ from *Hubble Space Telescope* (*HST*) Wide-Field Planetary Camera 2 (WFPC2) narrow-band imaging. In our model, the dust mass reaches this value at a burst age of $10^{7.25}$–$10^{7.5}$ yr. This age is consistent with the observationally suggested age of its major SF (e.g. Hunt et al. 2003). Cannon et al. (2002) obtained the extinction of $A_V = 0.5$ mag for some patches in this galaxy, which is reproduced by our model with the above age.

We show our model prediction for the SED of I Zw 18 in Fig. 10. We present the SED for the age $10^{7.25}$ yr and $10^{7.5}$ yr. The NIR flux measurements are taken from Hunt et al. (2003). I Zw 18 is not detected at all the four *IRAS* bands, hence we calculated the upper limits in the M–FIR from the sensitivity limits of *IRAS* observation. At 850 μm, the upper limit is converted from the data reported by Hunt, Bianchi & Maiolino (2005).

The IR luminosity is slightly smaller than the previous prediction of T03. We also find that the FIR peak wavelength is located at $\lambda \sim 60$ μm, shorter than that of the T03 model SED. In addition, the peak intensity is larger for the mixed model, as the mixed model produces about 30 per cent more dust than the unmixed model does (see Fig. 2). As the system still remains optically thin at this age because of the large $r_{\rm SF}$ value, this difference is directly reflected to the difference of the peak intensity.

The low opacity of I Zw 18 also leads to a low flux at N–MIR in the model SED in Fig. 10 both for unmixed and mixed cases compared with the T03 model SED. As mentioned by T03, the NIR continuum of I Zw 18 is expected to be dominated by stellar and nebular continuum radiation, and the contribution of dust may be negligible.

We expect that these features will be found commonly in young galaxies if they are optically thin in the IR. Hence, it may be useful to obtain some suggestions for the observational strategy of young galaxies at high z. We will discuss a well-known

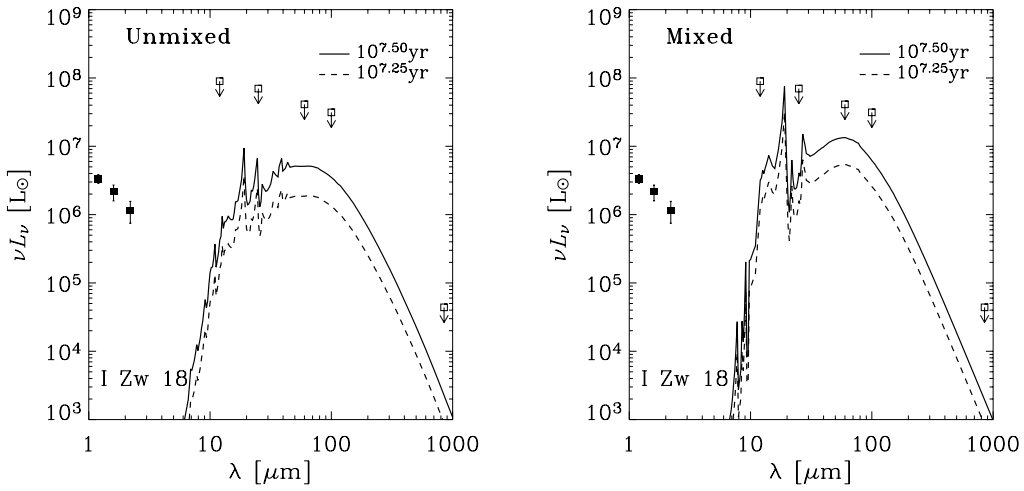

Figure 10. A prediction for the SED of a nearby 'quiescent' star-forming dwarf galaxy I Zw 18. We adopt SFR $= 0.04\,\mathrm{M}_\odot\,\mathrm{yr}^{-1}$ and $r_{\mathrm{SF}} = 100$ pc. The age of the SF is set to be $10^{7.25}$ yr (dashed lines) and $10^{7.5}$ yr (solid lines). As the NIR continuum of I Zw 18 is expected to be dominated by stellar and nebular continuum radiation, the contribution of dust may be negligible, and it is not necessary to reproduce these NIR observed fluxes by the present model.

real sample of such population of galaxies, LBGs, in the next subsection.

4.2 LBGs

LBGs are one of the most well-studied categories of high-z star-forming galaxies (e.g. Steidel et al. 1999, 2003). Even in LBGs, there is clear evidence that they contain a non-negligible amount of dust (e.g. Adelberger & Steidel 2000; Calzetti 2001). A high dust temperature ($\gtrsim$70 K) is suggested by subsequent studies (Ouchi et al. 1999; Chapman et al. 2000; Calzetti 2001; Sawicki 2001).

In order to make a consistent picture of the dust emission from LBGs, T04 applied the T03 model and made various predictions for these galaxies. They also considered a power-law dust size distribution to examine its effect on the resulting SEDs. The T04 model reproduced the known observational properties of the dust emission from LBGs.

In this paper, we investigate the expected appearance of the LBGs with the improved dust grain formation of N03.

4.2.1 Evolution of the SED of LBGs

We set the input parameters of the SED model for LBGs as follows. The SFR of LBGs spreads over the range of SFR $\simeq$ 1–300 $\mathrm{M}_\odot\,\mathrm{yr}^{-1}$ with a median of SFR $\simeq 20\,\mathrm{M}_\odot\,\mathrm{yr}^{-1}$ (e.g. Erb et al. 2003). A constant SFR up to the age of 10^9 yr is suggested to be a good approximation (e.g. Baker et al. 2004). Thus, the basic framework of the T03 model is also valid for LBGs. In this work, we consider the moderate case of SFR $= 30\,\mathrm{M}_\odot\,\mathrm{yr}^{-1}$ over the age of $10^{6.5}$–10^8 yr.

The most important information to calculate the IR SED is the effective size of the star-forming region, but it is the most uncertain quantity (see discussion of T04). As the mean half-light radius of LBGs is estimated to be $\sim$1.6 kpc from *HST* observations (Erb et al. 2003), we use the galaxy radius as the radius of a star-forming region, and set $r_{\mathrm{SF}} = 2$ kpc according to T04.

The SED evolution of LBGs is shown in Fig. 11. Note that the scale in the ordinate of Fig. 11 is different from those in Figs 4 and 5. Apart from luminosity, the behaviour of the SED evolution of LBG is qualitatively very similar to that of a dwarf-like forming galaxy with $r_{\mathrm{SF}} = 100$ pc (i.e. a weak NIR continuum and a strong M–FIR emission is commonly seen in both). This is because both the UV photon number density and dust number density are in the same order for an LBG and dwarf galaxy ($r_{\mathrm{SF}} = 100$ pc). As the IR luminosity depends on the dust column density, the total luminosity is different, but the shape of the SED is determined by the balance between the densities of UV photons and dust grains, they are similar with each other as for the shape.

The difference between the SEDs of the unmixed and mixed cases is small, and they give almost the same result especially in the M–FIR. This is explained as follows: the most prominent difference between the two is the N–MIR continuum, which is produced mainly by stochastic heating of grains. If the UV photon density is low, they are almost always in the lowest temperature state because the incidence of a UV photon is less frequent. In this case the N–MIR continuum from stochastically heated dust does not contribute to the continuum significantly, and the global SED shape is determined by larger grains in the equilibrium with the ambient UV radiation field. Under such a condition, they are similar in shape to each other. Thus, we see that it will be difficult to determine which scenario of dust production is correct from the observation of LBGs.

4.2.2 Observability of the dust emission from LBG

The flux density of a source at the observed frequency, ν_{obs} is obtained by

$$S_{\nu_{\mathrm{obs}}} = \frac{(1+z)L_{(1+z)\nu_{\mathrm{obs}}}}{4\pi d_{\mathrm{L}}(z)^2} = \frac{(1+z)L_{\nu_{\mathrm{em}}}}{4\pi d_{\mathrm{L}}(z)^2} \quad (3)$$

where $d_{\mathrm{L}}(z)$ is the luminosity distance corresponding to a redshift z, and ν_{obs} and ν_{em} are the observed and emitted frequency, respectively.

We show the observed IR/submm SEDs of LBGs at $z = 2$, 3 and 4 in Fig. 12. For simplicity we only show the SED with the age of 10^8 yr. The thick black short horizontal lines indicate the 3σ detection limits for an 8-h observation by ALMA (Atacama Large Millimeter Array).[4] Here we assumed 64 antennas and three wavelength bands, 450, 850 and 1080 μm. We also show the 3σ source confusion limit of *Herschel*[5] at 75-, 160-, 250- and 350-μm

[4] URL: http://www.alma.info/

[5] URL: http://www.rssd.esa.int/herschel/

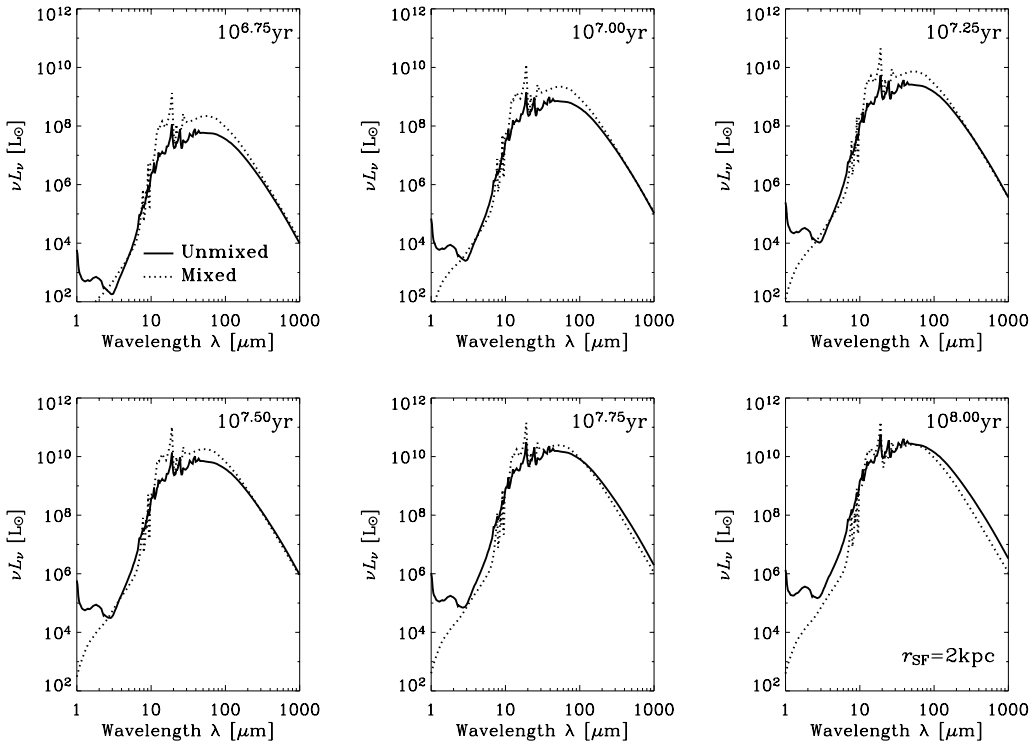

Figure 11. The evolution of the SED of a typical LBG. The SFR is set to be SFR $= 30\,\mathrm{M}_\odot\,\mathrm{yr}^{-1}$, and the size of the star-forming region $r_{\mathrm{SF}} = 2\,\mathrm{kpc}$.

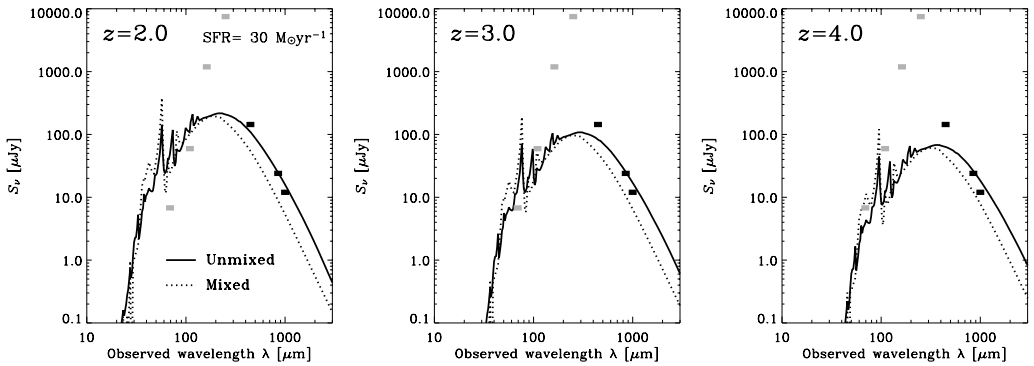

Figure 12. The expected flux densities of an LBG. In this figure we set the galaxy burst age of $t = 10^8$ yr. Confusion limits of *Herschel* and detection limits of ALMA 8-h survey are also shown by grey and black thick horizontal lines, respectively.

bands by thick grey horizontal lines. These limits are based on 'the photometric criterion' of (Lagache, Dole & Puget 2003). See also Ishii, Takeuchi & Sohn (2002) and Takeuchi & Ishii (2004a).

As discussed in T04, the detectability of LBGs is not strongly dependent on their redshifts. The predicted IR luminosity is factor of 2 smaller than that of T04, hence it is more difficult to detect LBGs than the discussion in T04: we need roughly four times longer an integration time than that derived from T04, if we fix all the other conditions. Detection at 350 μm seems impossible for moderate-SFR LBGs. However, at longer wavelengths, for ages $\gtrsim 10^8$ yr and SFR $\gtrsim 30\,\mathrm{M}_\odot\,\mathrm{yr}^{-1}$, LBGs can be detected at a wide range of redshifts in the submm by the ALMA deep survey. In the FIR, *Herschel* will detect the dust emission from LBGs at $z \simeq 2$, but it is difficult at higher z values. As the SED does not differ for the unmixed or mixed dust formation, our evaluation of the observability of LBGs holds both for the mixed and unmixed dust formation.

4.3 Toward higher redshifts

Based on the previous discussions, we give a brief consideration on the observation of very high-z galaxies ($z \gtrsim 5$) here. Direct observation of such galaxies are of vital importance to explore the physics of galaxy formation.

First, assume a LBG at these redshifts. Fig. 13 shows such a situation. We assumed the same physical parameters for LBGs. From Fig. 13, we find that LBG-like objects can be detectable even at $z \simeq 10$ if SFR $\gtrsim 30\,\mathrm{M}_\odot\,\mathrm{yr}^{-1}$. At $z \simeq 20$, it may be more difficult, but might be possible to detect LBGs with very high SFR, by an ALMA ultra-deep survey with a much longer integration time than 8 h.

However, it may not be reasonable to assume galaxy-like LBGs at $z \simeq 10$ because they are rather massive system in general ($M_{\mathrm{star}} \simeq 10^{10}\,\mathrm{M}_\odot$), and, from a modern cosmological viewpoint, such a massive system is very rare with such a high-z, young universe.

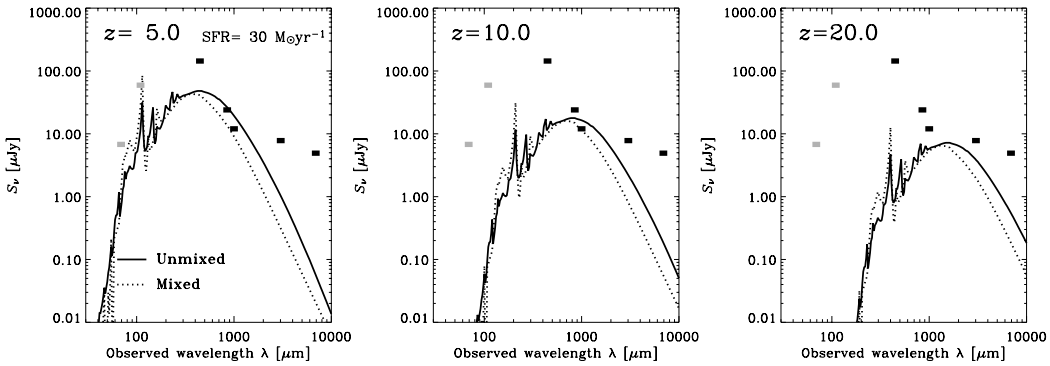

Figure 13. The expected flux densities of an LBGs hypothetically located at $z = 5$, 10 and 20. The assumed parameters are the same as those for Fig. 12. The solid lines represent the SEDs for the unmixed case of dust production, and dotted lines for the mixed case. We put the same observational detection limits as in Fig. 12 for *Herschel* and ALMA.

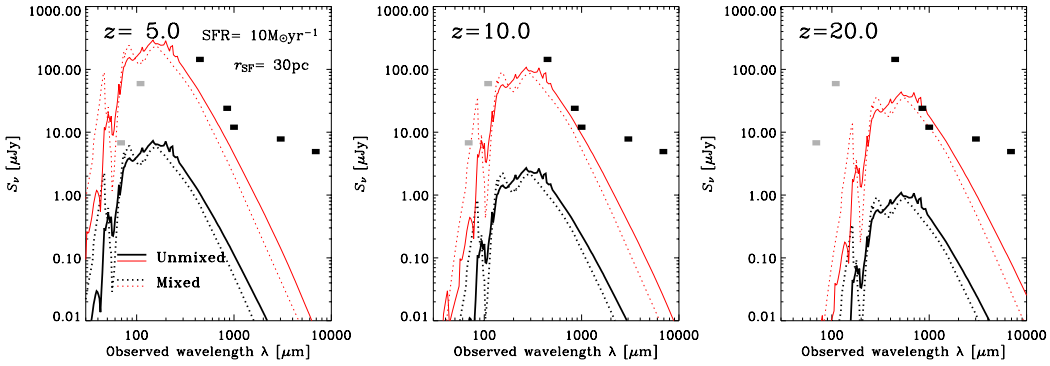

Figure 14. The expected flux densities of a dwarf star-forming galaxy located at $z = 5$, 10 and 20. The solid lines represent the SEDs for the unmixed case of dust production, and the dotted lines for the mixed case. We assumed SFR $= 10\,\mathrm{M}_\odot\,\mathrm{yr}^{-1}$ and $r_{\rm SF} = 30\,\mathrm{pc}$. The thick lines are the expected SEDs for an unlensed galaxy, while the thin lines are the ones for a gravitationally lensed galaxy by a magnification factor of 40. Again the detection limits are the same as those of Fig. 12.

Here we discuss an object less massive than LBGs. In modern hierarchical structure formation scenarios, it would be more reasonable to assume a small, subgalactic clump as a first forming galaxy. Consider a dark halo of mass $\sim 10^9\,\mathrm{M}_\odot$, it is then expected to contain a gas with mass $\simeq 10^8\,\mathrm{M}_\odot$. For this purpose, we calculate the SEDs for a dwarf star-forming galaxy. If gas collapses on the free-fall time-scale with an efficiency of $\epsilon_{\rm SF}$ (we assume $\epsilon_{\rm SF} = 0.1$), we obtain the following evaluation of the SFR Hirashita & Hunt (2004):

$$\mathrm{SFR} \simeq 0.1 \left(\frac{\epsilon_{\rm SF}}{0.1}\right) \left(\frac{M_{\rm gas}}{10^7\,\mathrm{M}_\odot}\right) \left(\frac{n_{\rm H}}{100\,\mathrm{cm}^{-3}}\right)^{1/2} [\mathrm{M}_\odot\ \mathrm{yr}^{-1}] \quad (4)$$

and

$$n_{\rm H} \simeq 100 \left(\frac{r_{\rm SF}}{100\,\mathrm{pc}}\right)^{-3} \left(\frac{M_{\rm gas}}{10^7\,\mathrm{M}_\odot}\right) [\mathrm{cm}^{-3}], \quad (5)$$

where $n_{\rm H}$ is the hydrogen number density. Then we have

$$\mathrm{SFR} \simeq 0.1 \left(\frac{\epsilon_{\rm SF}}{0.1}\right) \left(\frac{M_{\rm gas}}{10^7\,\mathrm{M}_\odot}\right)^{3/2} \left(\frac{r_{\rm SF}}{100\,\mathrm{pc}}\right)^{-3/2} [\mathrm{M}_\odot\ \mathrm{yr}^{-1}]\,. \quad (6)$$

If we consider $M_{\rm gas} \simeq 10^8\,\mathrm{M}_\odot$, we have SFR $\simeq 3(r_{\rm SF}/100\,\mathrm{pc})^{-3/2}\,\mathrm{M}_\odot\,\mathrm{yr}^{-1}$. In addition, as we see below, an extremely high-z galaxy observed by *HST* has a very compact morphology (Kneib et al. 2004). We also mention that, from a theoretical side, high-z galaxies are suggested to be dense and compact compared to nearby galaxies (Norman & Spaans 1997; Hirashita & Ferrara 2002). Hence, it may be reasonable to assume a same type of galaxy as local dwarfs discussed in Section 4.2.1. Thus, we consider a dwarf galaxy with SFR $= 10\,\mathrm{M}_\odot\,\mathrm{yr}^{-1}$ as an example, and we adopt $r_{\rm SF} = 30$ and 100 pc. The age is set to be 10^7 yr. If the age is older, they will become easier to detect if a constant SFR takes place. We show the expected SEDs for such galaxies at $z = 5$, 10 and 20 in Figs 14 and 15. As expected, it seems almost impossible to detect such objects by *Herschel* or ALMA.

There is, however, the possibility of observing such a small forming galactic clump directly: gravitational lensing works very well as a natural huge telescope. For example, MS 1512−cB58 is an ideal case of a lensed LBG (Nakanishi et al. 1997; Baker et al. 2004), and more recently, a small star-forming galaxy has been detected by *HST* and *Spitzer* observations (Kneib et al. 2004; Egami et al. 2005). Hence, we can expect a forming galaxy which is intrinsically small and faint but magnified by a gravitational potential of a cluster of galaxies. If we assume a lens magnification factor of 40, such a small galaxy becomes detectable. This is depicted by the thin lines in Figs 14 and 15. As the expected SED of such a compact dwarf galaxy has a strong MIR continuum at their rest frame, it can be feasible to detect at the FIR in the observed frame. Indeed, at $z = 5$ they appear above the confusion limits of *Herschel*. As the confusion limit of *Herschel* may be, in fact, very difficult to reach in actual observations, a cooled FIR space telescope is more suitable for such observation, and this will be a strong scientific

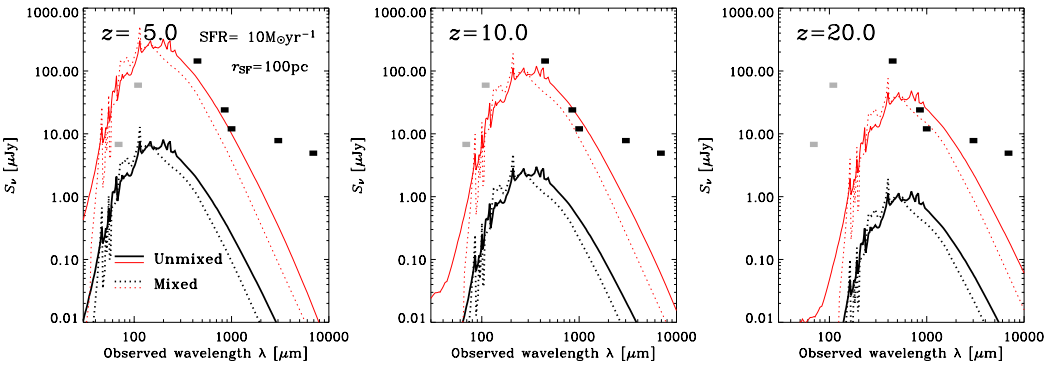

Figure 15. The same as Fig. 14, except that $r_{\rm SF} = 100\,{\rm pc}$.

motivation for a future project like *SPICA*.[6] In the FIR wavelength regime (50–200 μm), the SEDs of unmixed and mixed cases might be distinguishable. If FIR spectroscopy is performed, the picture of dust production is plausible might be examined. At higher z values, they can be detected by the ALMA survey. Even at $z \simeq 20$, they can be detected by a standard 8-h survey of ALMA, if lensing takes place. It is interesting to note that, at $z \simeq 10$, the peak of their SED happens at the wavelength range where the detection limits of both *Herschel* and ALMA are not very good. A new effective (probably space) facility should be developed to overcome this observational difficulty.

With this line of study, we must estimate how frequently such lensing events occur for high-z objects. Suppose a cluster of galaxies at $z_{\rm l} \simeq 0.1$–0.2 whose dynamical mass $M_{\rm dyn}$ is $5 \times 10^{14}\,{\rm M}_\odot$ and whose mass distribution obeys the singular isothermal sphere. We denote the strong lensing cross section, i.e. the area of the region in the source plane for which the resulting magnification by a cluster is larger than μ, as $\sigma(>\mu)$. Perrotta et al. (2002) presented $\sigma(>\mu)$ as a function of $M_{\rm dyn}$ for $z_{\rm lens} = 1.0$. As $\sigma(>\mu) \propto {D_{\rm ls}}^2$ [$D_{\rm ls}$ is the angular-diameter distance between the lens and the source (e.g. Asada 1998)] (Covone, Sereno & de Ritis 2005), we can convert their result to our condition and obtain $\sigma(>10) \simeq 30\,{\rm arcsec}^2$ on the source plane.[7] This result is almost independent of the source redshifts. Setting the limiting flux density $S_\nu = 1$ μJy and using the number counts of Hirashita & Ferrara (2002) for galaxies at $z > 5$, we have an expected number of galaxies suffering a strong lensing of $\simeq$1–3. Thus, we expect at least a few strongly lensed IR galaxies to this survey depth.

To have a concrete idea for the observational strategy, we must consider an important aspect of the lensing. It is known that the gravitational lensing affects the galaxy number counts in two opposite directions: (i) it magnifies the flux density of galaxies; and (ii) it stretches the sky area and decreases their number density on the sky. This is called the 'magnification bias' (Fort, Mellier & Dantel-Fort 1997; Bézecourt, Pelló & Soucail 1998). The unlensed number count $N_0(>S_\nu)$ is generally approximated by a power law

$$N_0(>S_\nu) \propto {S_\nu}^{\beta}. \tag{7}$$

Then, by denoting the magnification factor as μ, we obtain the lensed number counts $N_{\rm lens}\,(>S_\nu)$ as

$$N_{\rm lens}(>S_\nu) = N_0(>S_\nu)\mu^{-(\beta+1)} \tag{8}$$

(e.g. Fort, Mellier & Dantel-Fort 1997; Takeuchi, Yoshikawa & Yonehara 2000). Equation (8) shows that whether the number counts increases or decreases depends on the slope of the counts, β: if $\beta < -1$ lensing works as an enhancement of the counts. As the slope of the number counts of such galaxies is expected to be steeper than -1 (e.g. Hirashita & Ferrara 2002), the source density on the image plane will increase (see also Perrotta et al. 2002). Thus, we are confident that the lensing will work as a really useful tool to detect small galaxies forming via dust emission.

5 CONCLUSION

Dust plays various important roles even in the very early phase of galaxy evolution (e.g. Hirashita & Ferrara 2002). In such a young phase with a typical age less than 10^9 yr, dust is predominantly supplied by SNe. With the aid of a new physical model of dust production by SNe developed by N03, we constructed a model of dust emission from very young galaxies according to T03.

N03 carefully took into account the radial density profile and the temperature evolution in the calculation of the dust formation in the ejecta of SNe II and PISNe. They also showed that the produced dust species depends strongly on the mixing within SNe. We treated both unmixed and mixed cases and calculated the IR SED of young galaxies for both cases.

The SEDs constructed from N03 dust production are less luminous than those by T03 model by a factor of 2–3. This difference is due to the improvement in the treatment of $Q(a, \lambda)$ at UV and the considered grain species. The SED for the unmixed case is found to have a strong N–MIR continuum radiation in its early phase of the evolution (age $\lesssim 10^{7.25}$ yr) compared with that for the mixed case. The N–MIR continuum is due to the emission from silicon grains, which only exist in the species of the unmixed dust production.

We also calculated the IR extinction curves for young galaxies. N03 dust gives a weaker extinction than that of T03 model because of the small relative number of very small dust grains. This is also the cause of the smaller IR luminosity of the present model. For the unmixed case, NIR extinction is dominated by large grains of silicon and amorphous carbon, and silicate features are less prominent compared to the curve given by T03. In contrast, the extinction curve of the mixed case has a similar shape to that of T03.

The SED of a local starbursting dwarf galaxy, SBS 0335−052, was calculated. Recent *Spitzer* observations (Houck et al. 2004) have implied a hotter dust than previously thought. Our present model SED naturally reproduces the strong N–MIR continuum and the lack of cold FIR emission of SBS 0335−052. We found that only the SED

[6] URL: http://www.ir.isas.jaxa.jp/SPICA/index.html
[7] On the image plane, the area corresponds to $\simeq \mu\sigma(>\mu)$.

of the unmixed case can reproduce the N–MIR continuum of this galaxy. Hence, as for SBS 0335−052, the unmixed dust production is preferred. It will be interesting to proceed this line of study for higher-z galaxies.

A prediction for the SED of another typical nearby star-forming dwarf galaxy, I Zw 18, was then made. As I Zw 18 is dominated by very young SF, we may adopt the model to this galaxy. Using the dust species from N03 with this model, we find a weaker FIR emission than that of T03. The N–MIR continuum is also expected to be much weaker than that of T03 SED.

We also calculated the evolution of the SED of LBGs. For the parameters of LBGs, the unmixed and mixed picture does not affect the appearance of the SED. Hence, if we combine our model with the knowledge obtained from optical observations, the observability of LBGs at submm wavelengths are robust enough independent of the details of the SNe dust production theory.

Finally, we considered the observations of forming galaxies at $z \gtrsim 5$. If there exist LBG-like galaxies at these redshifts, they can be detected at $z \lesssim 10$ by the ALMA 8-h survey if SFR $\gtrsim 30\,\mathrm{M}_\odot\,\mathrm{yr}^{-1}$. For small forming galaxies or subgalactic clumps, it is almost impossible to detect their intrinsic flux by ALMA or by *Herschel*. However, the gravitational lensing is found to be a very effective tool to detect such small star-forming galaxies at $z \gtrsim 5$. If we consider a compact dwarf galaxy with SFR $\simeq 10\,\mathrm{M}_\odot\,\mathrm{yr}^{-1}$ and $r_{\mathrm{SF}} \simeq 30\,\mathrm{pc}$, we can expect a few strongly magnified galaxies behind a typical cluster of galaxies at $z \simeq 0.1$–0.2.

ACKNOWLEDGMENTS

First we are grateful to the anonymous referee for many insightful comments which have improved the clarity of this paper so much. We deeply thank Akio K. Inoue, Jean-Paul Kneib and Giovanni Covone for illuminating discussions. We made extensive use of the NASA Astrophysics Data System. TTT, TTI and HH have been supported by the Japan Society of the Promotion of Science. TK is supported by a Grant-in-Aid for Scientific Research from JSPS (16340051).

REFERENCES

Adelberger K. L., Steidel C. C., 2000, ApJ, 544, 218
Arendt R. G., Dwek E., Moseley S. H., 1999, ApJ, 521, 234
Arnett W. D., Bahcall J. N., Kirshner R. P., Woosley S. E., 1989, ARA&A, 27, 629
Asada H., 1998, ApJ, 501, 473
Baker A. J., Tacconi L. J., Genzel R., Lehnert M. D., Lutz D., 2004, ApJ, 604, 125
Begemann B., Dorschner J., Henning T., Mutschke H., Thamm E., 1994, ApJ, 423, L71
Bertoldi F., Carilli C. L., Cox P., Fan X., Strauss M. A., Beelen A., Omont A., Zylka R., 2003, A&A, 406, L55
Bézecourt J., Pelló R., Soucail G., 1998, A&A, 330, 399
Bohren C. F., Huffman D. R., 1983, Absorption and Scattering of Light by Small Particles. Wiley, New York
Bouwens R. J. et al., 2004a, ApJ, 606, L25
Bouwens R. J. et al., 2004b, ApJ, 616, L79
Calzetti D., 2001, PASP, 113, 1449
Calzetti D., Armus L., Bohlin R. C., Kinney A. L., Koornneef J., Storchi-Bergmann T., 2000, ApJ, 533, 682
Cannon J. M., Skillman E. D., Garnett D. R., Dufour R. J., 2002, ApJ, 565, 931
Chapman S. C. et al., 2000, MNRAS, 319, 318
Covone G., Sereno M., de Ritis R., 2005, MNRAS, 357, 773
Dale D. A., Helou G., Neugebauer G., Soifer B. T., Frayer D. T., Condon J. J., 2001, AJ, 122, 1736
Dorschner J., Begemann B., Henning Th., Jaeger C., Mutschke H., 1995, A&A, 300, 503
Douvion T., Lagage P. O., Cesarsky C. J., Dwek E., 2001, A&A, 373, 281
Draine B. T., Anderson L., 1985, ApJ, 292, 494
Draine B. T., Lee H. M., 1984, ApJ, 285, 89
Draine B. T., Li A., 2001, ApJ, 551, 807
Dunne L., Eales S., Ivison R., Morgan H., Edmunds M., 2003, Nat, 424, 285
Dwek E., 1998, ApJ, 501, 643
Dwek E., 2004, ApJ, 607, 848
Dwek E., Scalo J. M., 1980, ApJ, 239, 193
Eales S., Bertoldi F., Ivison R., Carilli C., Dunne L., Owen F., 2003, MNRAS, 344, 169
Edo O., 1983, PhD thesis, Univ. Arizona
Edward D. F., 1985, in Palik E. D., ed., Handbook of Optical Constants of Solids. Academic Press, San Diego, p. 547
Egami E. et al., 2005, ApJ, 618, L5
Erb D. K., Shapley A. E., Steidel C. C., Pettini M., Adelberger K. L., Hunt M. P., Moorwood A. F. M., Cuby J.-G., 2003, ApJ, 591, 101
Feder J., Russell K. C., Lothe J., Pound M., 1966, Adv. Phys., 15, 111
Fort B., Mellier Y., Dantel-Fort M., 1997, A&A, 321, 353
Gail H.-P., Sedlmayr E., 1979, A&A, 77, 165
Gail H.-P., Keller R., Sedlmayr E., 1984, A&A, 133, 320
Galliano F., Madden S. C., Jones A. P., Wilson C. D., Bernard J.-P., Le Peintre F., 2003, A&A, 407, 159
Galliano F., Madden S. C., Jones A. P., Wilson C. D., Bernard J.-P., 2005, A&A, 434, 867
Green D. A., Tuffs R. J., Popescu C. C., 2004, MNRAS, 355, 1315
Grønvold F., Stølen S., Labban A. K., Westrum E. F., Jr, 1991, J. Chem. Thermodyn., 23, 261
Hama J., Suito K., 1999, Phys. Earth Planet. Interiors, 114, 165
Heger A., Woosley S. E., 2002, ApJ, 567, 532
Hines D. C. et al., 2004, ApJS, 154, 290
Hirashita H., Ferrara A., 2002, MNRAS, 337, 921
Hirashita H., Hunt L. K., 2004, A&A, 421, 555
Hirashita H., Hunt L. K., Ferrara A., 2002, MNRAS, 330, L19
Hirashita H., Nozawa T., Kozasa T., Ishii T. T., Takeuchi T. T., 2005, MNRAS, 357, 1077
Houck J. R. et al., 2004, ApJS, 154, 211
Hughes D. H. et al., 1998, Nat, 394, 241
Hunt L. K., Vanzi L., Thuan T. X., 2001, ApJ, 377, 66
Hunt L. K., Giovanardi C., Helou G., 2002, A&A, 394, 873
Hunt L. K., Thuan T. X., Izotov Y. I., 2003, ApJ, 2003,588, 281
Hunt L. K., Dyer K. K., Thuan T. X., Ulvestad J. S., 2004, ApJ, 606, 853
Hunt L. K., Bianchi S., Maiolino R., 2005, A&A, 434, 849
Inoue A. K., 2005, MNRAS, 359, 171
Inoue A. K., Hirashita H., Kamaya H., 2000, PASJ, 52, 539
Ishii T. T., Takeuchi T. T., Sohn J.-J., 2002, in Giard M. et al., eds, Infrared and Submillimeter Space Astronomy: An International Colloquium to Honor the Memory of Guy Serra., EDP Sciences, Les Wis, p. 169
Jäger C., Dorschner J., Mutschke H., Posch Th., Henning Th., 2003, A&A, 408, 193
Jones A. P., Tielens A. G. G. M., Hollenbach D. J., 1996, ApJ, 469, 740
Joy M., Lester D. F., 1988, ApJ, 331, 1451
Kneib J., Ellis R. S., Santos M. R., Richard J., 2004, ApJ, 607, 697
Krause O., Birkmann S. M., Rieke G. H., Lemke D., Klaas U., Hines D. C., Gordon K. D., 2004, Nat, 432, 596
Kozasa T., Hasegawa H., 1987, Prog. Theor. Phys., 77, 1402
Kozasa T., Hasegawa H., Nomoto K., 1989, ApJ, 344, 325
Krügel E., 2003, The Physics of Interstellar Dust. IOP Publishing, Bristol
Lagache G., Dole H., Puget J.-L., 2003, MNRAS, 338, 555
Ledoux C., Bergeron J., Petitjean P., 2002, A&A, 385, 802
Ledoux C., Petitjean P., Srianand R., 2003, MNRAS, 346, 209
Lilly S. J., Le Fèvre O., Hammer F., Crampton D., 1996, ApJ, 460, L1

Lynch D. W., Hunter W. R., 1991, in Palik E. D., ed., Handbook of Optical Constants of Solids II. Academic Press, San Diego, p. 388
Madau P., Ferguson H. C., Dickinson M. E., Giavalisco M., Steidel C. C., Fruchter A., 1996, MNRAS, 283, 1388
Maiolino R., Schneider R., Oliva E., Bianchi S., Ferrara A., Mannucci F., Pedani M., Roca Sogorb M., 2004, Nat, 431, 533
Mezzasalma S. A., 2000, J. Phys. Chem. Solids, 61, 593
Morgan H. L., Edmunds M. G., 2003, MNRAS, 343, 427
Morgan H. L., Dunne L., Eales S. A., Ivison R. J., Edmunds M. G., 2003, ApJ, 597, L33
Mukai T., 1989, in Bonetti A., Greenberg J. M., Aiello S., eds, Evolution of Interstellar Dust and Related Topics. Elsevier Science, Amsterdam, p. 397
Nakanishi K., Ohta K., Takeuchi T. T., Akiyama M., Yamada T., Shioya Y., 1997, PASJ, 49, 535
Norman C. A., Spaans M., 1997, ApJ, 480, 145
Nozawa T., Kozasa T., Umeda H., Maeda K., Nomoto K., 2003, ApJ, 598, 785 (N03)
Oganov A. R., Brodholt J. P., Price G. D., 2000, Phys. Earth Planet. Interiors, 122, 277
Östlin G., 2000, ApJ, 535, L99
Ouchi M., Yamada T., Kawai H., Ohta K., 1999, ApJ, 517, L19
Perrotta F., Baccigalupi C., Bartelmann M., De Zotti G., Granato G. L., 2002, MNRAS, 329, 445
Philipp H. R., 1985, in Palik E. D., ed., Handbook of Optical Constants of Solids. Academic Press, San Diego, p. 719
Plante S., Sauvage M., 2002, AJ, 124, 1995
Roessler D. M., Huffman D. R., 1991, in Palik E. D., ed., Handbook of Optical Constants of Solids II. Academic Press, San Diego, p. 919
Salpeter E., 1955, ApJ, 121, 161
Sawicki M., 2001, AJ, 121, 2405
Schaerer D., 2002, A&A, 382, 28
Schneider R., Ferrara A., Salvaterra R., 2004, MNRAS, 351, 1379
Semenov D., Henning Th., Helling Ch., Ilgner M., Sedlmayr E., 2003, A&A, 410, 611
Shepherd J. P., Koenitzer J. W., Aragón R., Spalek J., Honig J. M., 1991, Phys. Rev. B, 43, 8461
Siethoff H., Ahlborn K., 1996, J. Appl. Phys., 79, 2968
Stanway E. R., Bunker A. J., McMahon G., 2003, MNRAS, 342, 439
Steidel C. C., Giavalisco M., Pettini M., Dickinson M., Adelberger K. L., 1996, ApJ, 462, L17
Steidel C. C., Adelberger K. L., Giavalisco M., Dickinson M., Pettini M., 1999, ApJ, 519, 1
Takeuchi T. T., Ishii T. T., 2004a, ApJ, 604, 40
Takeuchi T. T., Ishii T. T., 2004b, A&A, 426, 425 (T04)
Takeuchi T. T., Yoshikawa K., Yonehara A., 2000, in Matsumoto T., Shibai H., eds, ISAS Report SP-14, Mid- and Far-Infrared Astronomy and Space Missions, ISAS, Sagamihara, p. 163
Takeuchi T. T., Ishii T. T., Hirashita H., Yoshikawa K., Matsuhara H., Kawara K., Okuda H., 2001a, PASJ, 53, 37
Takeuchi T. T., Kawabe R., Kohno K., Nakanishi K., Ishii T. T., Hirashita H., Yoshikawa K., 2001b, PASP, 113, 586
Takeuchi T. T., Hirashita H., Ishii T. T., Hunt L. K., Ferrara A., 2003a, MNRAS, 343, 839 (T03)
Takeuchi T. T., Yoshikawa K., Ishii T. T., 2003b, ApJ, 587, L89
Takeuchi T. T., Buat V., Iglesias-Páramo J., Boselli A., Burgarella D., 2005, A&A, 432, 423
Tanaka K. K., Tanaka H., Nakazawa K., 2002, Icarus, 160, 197
Tinsley B. M., Danly L., 1980, ApJ, 242, 435
Todini P., Ferrara A., 2001, MNRAS, 325, 726 (TF01)
Toon O. B., Pollack J. B., Khare B. N., 1976, J. Geophys. Res., 81, 5733
Totani T., Takeuchi T. T., 2002, ApJ, 570, 470
Umeda H., Nomoto K., 2002, ApJ, 565, 385
Vanzi L., Hunt L. K., Thuan T. X., Izotov Y. I., 2000, A&A, 363, 493
Whittet D. C. B., 1992, Dust in the Galactic Environment, IOP, New York
Wilson T. L., Batrla W., 2005, A&A, 430, 561

APPENDIX A: DETAILS OF THE CHEMICAL EVOLUTION

Here we present a detailed description of the chemical evolution used in this work. Full treatment of the present chemical evolution model including the feedback, dust destruction and more complex SF history is given elsewhere (Nozawa et al., in preparation). Within the framework of the closed-box model, the total baryonic mass of a galaxy, $M_{\rm T}$, is conserved as

$$M_{\rm T} = M_{\rm gas}(0) = M_{\rm gas}(t) + M_{\rm dust}(t) + M_{\rm star}(t) + M_{\rm rem}(t), \qquad \text{(A1)}$$

where $M_{\rm gas}(t)$ is the gas mass, $M_{\rm dust}(t)$ is the dust mass, $M_{\rm star}(t)$ is the stellar mass and $M_{\rm rem}(t)$ is the mass of stellar remnants in the galaxy at an age of t. We start the calculation from homogeneous pristine gas, i.e. $M_{\rm dust}(0) = M_{\rm star}(0) = M_{\rm rem}(0) = 0$. The time evolution of the mass of interstellar medium, $M_{\rm ISM}(t) \equiv M_{\rm gas}(t) + M_{\rm dust}(t)$ is given by

$$\left.\frac{{\rm d}M_{\rm ISM}}{{\rm d}t}\right|_t = -\psi(t) + \int_{m_{\rm l}}^{m_{\rm u}} [m - m_{\rm rem}(m)]\,\psi(t-\tau_m)\phi(m){\rm d}m, \qquad \text{(A2)}$$

where $\psi(t)$ is the SFR at age t, $\phi(m)$ is the IMF normalized to unity in the mass interval $[m_{\rm l}, m_{\rm u}]$ (subscripts l and u mean lower and upper mass limit, respectively), $m_{\rm rem}(m)$ is the mass of a single stellar remnant resulting from a progenitor star with mass m and τ_m is the lifetime of a star with mass m.

For the IMF, as we mentioned in the main text, we adopt the Salpeter IMF with mass range of $(m_{\rm l}, m_{\rm u}) = (0.1\,{\rm M}_\odot, 100\,{\rm M}_\odot)$. The lifetime τ_m is evaluated by a fitting formula of zero-metallicity tracks with no mass loss, given by Schaerer (2002). For SNe II (progenitor mass 8–40 $\rm M_\odot$), we approximate the remnant mass $m_{\rm rem}$ by the linear fit based on the numerical result of SN explosions given by Umeda & Nomoto (2002)

$$m_{\rm rem}(m) = 0.06m + 0.93 (8 < m < 40\,{\rm M}_\odot). \qquad \text{(A3)}$$

For other progenitor mass ranges, we set $m_{\rm rem}(m) = 0$ at $m < 8\,{\rm M}_\odot$ (no remnants), and $m_{\rm rem}(m) = m$ at $40\,{\rm M}_\odot < m < 100\,{\rm M}_\odot$ (all the mass is swallowed by a black hole). In this work, we do not treat PISNe in the calculation. By equation (A3), the time evolution of $M_{\rm rem}(t)$ is expressed by

$$\left.\frac{{\rm d}M_{\rm rem}}{{\rm d}t}\right|_t = \int_{m_{\rm l}}^{m_{\rm u}} m_{\rm rem}(m)\psi(t-\tau_m)\phi(m){\rm d}m. \qquad \text{(A4)}$$

The time evolution of $M_{\rm dust}(t)$ is, then, obtained as

$$\left.\frac{{\rm d}M_{\rm dust}}{{\rm d}t}\right|_t = -\frac{M_{\rm dust}(t)}{M_{\rm ISM}(t)}\psi(t) + \int_{m_{\rm l}}^{m_{\rm u}} m_{\rm dust}(m)\psi(t-\tau_m)\phi(m){\rm d}m \qquad \text{(A5)}$$

where $m_{\rm dust}(m)$ denotes the dust mass produced by a progenitor with mass m. We apply the dust formation model of N03 for $m_{\rm dust}$. As we mentioned in Section 2.1, we used the result of progenitor mass $20\,{\rm M}_\odot$ for the fraction and the size distribution of dust grain species, hence the mass fraction and size distribution are constant in time along with the evolution.

APPENDIX B: NORMALIZATION OF THE NUMBER DENSITY OF GRAIN SPECIES

In this Appendix, we show how to obtain the normalization of the dust size distribution ${\rm d}N_i/{\rm d}a_i$

$$\frac{{\rm d}N_i}{{\rm d}a}{\rm d}a \equiv A f_i(a)\,{\rm d}a \qquad \text{(B1)}$$

where subscript i denotes the species of dust, and f_i is the mass fraction of dust of species i, given by N03, and A is the normalization constant. We denote the material density of i-species dust by ρ_i, and the SF region radius as $r_{\rm SF}0$. The total mass of dust species i, M_i, is then written as

$$M_i = \rho_i \int \frac{4\pi a^3}{3} \frac{{\rm d}N_i}{{\rm d}a}\,{\rm d}a = \rho_i \int \frac{4\pi a^3}{3} A f_i(a)\,{\rm d}a$$
$$= \frac{4\pi A}{3}\rho_i \int a^3 f_i(a)\,{\rm d}a. \quad \text{(B2)}$$

The total dust mass of all the species, M, is

$$M = \sum_i \frac{4\pi A}{3}\rho_i \int f_i(a) a^3\,{\rm d}a = \frac{4\pi A}{3}\sum_i \rho_i \int f_i(a) a^3\,{\rm d}a\ . \quad \text{(B3)}$$

Hence

$$A = \frac{3M}{4\pi \sum_i \rho_i \int f_i(a) a^3\,{\rm d}a}\ . \quad \text{(B4)}$$

Thus we can determine A from the available data. Note that only M depends on time t, hence the time dependence of A is given only through M. The total number of grains, N_i, is expressed as

$$N_i = \int \frac{{\rm d}N_i}{{\rm d}a_i}\,{\rm d}a_i. \quad \text{(B5)}$$

This paper has been typeset from a TEX/LATEX file prepared by the author.